Effective Connectivity in Default Mode Network for Alcoholism Diagnosis

Danish M. Khan, *Student Member, IEEE*, Norashikin Yahya, *Member, IEEE*, Nidal Kamel, *Senior Member, IEEE*, and Ibrahima Faye, *Senior Member, IEEE*

***Abstract*— Alcohol Use Disorder (AUD) is a chronic relapsing brain disease characterized by excessive alcohol use, loss of control over alcohol intake, and negative emotional states under no alcohol consumption. The key factor in successful treatment of AUD is the accurate diagnosis for better medical and therapy management. Conventionally, for individuals to be diagnosed with AUD, certain criteria as outlined in the Diagnostic and Statistical Manual of Mental Disorders (DSM) should be met. However, this process is subjective in nature and could be misleading due to memory problems and dishonesty of some AUD patients. In this paper, an assessment scheme for objective diagnosis of AUD is proposed. For this purpose, EEG recording of 31 healthy controls and 31 AUD patients are used for the calculation of effective connectivity (EC) between the various regions of the brain Default Mode Network (DMN). The EC is estimated using partial directed coherence (PDC) which are then used as input to a 3D Convolutional Neural Network (CNN) for binary classification of AUD cases. Using 5-fold cross validation, the classification of AUD vs. HC effective connectivity matrices using the proposed 3D-CNN gives an accuracy of 87.85 ± 4.64 %. For further validation, 32 and 30 subjects are randomly selected for training and testing, respectively, giving 100% correct classification of all the testing subjects.**

***Index Terms*— 3D Convolutional neural networks, alcohol use disorder, alcoholism, default mode network, brain effective connectivity, deep learning, multivariate autoregressive models, partial directed coherence.**

I. Introduction

ACCORDING to the reports published by the LANCET [1] and NATURE [2], about 5% of global burden of diseases is attributed to excessive alcohol consumption and corresponds to 6% of total deaths that occur annually. Besides, it has been established in [3], that the adverse effects of alcohol far exceed those due to illicit drugs. An alcohol-addict may be regarded as a heavy drinker who consumes ethanol >100 g/day for males and >60 g/day for females [4]. In European countries, this population accounts for 0.8% of people aged between 15 to 65 years old, with around half diagnosed with liver cirrhosis and shorten life expectancy by 25 to 31 years [2]. Long-term excessive drinking can be damaging to human brain as it can diminish the brain's gray and white matter [5]. Similarly, in short-term, alcohol may debilitate many brain functionalities which may result in issues like memory loss and confabulation, black out, recklessness, enfeebled decision making, diminished perspicacity, visuo-spatial enervation, Wernicke–Korsakoff syndromes and attention deficiency [6].

Grant et.al analyzed data collected by national epidemiologic survey on alcohol and related conditions III (NESARC-III) and found that only 19.8% of AUD patients opt for some treatment in their lifetime [7]. Additionally, the time between filing a diagnostic criterion and receiving a proper treatment is also very long. This lag may be attributed to the improper diagnosis, lack of availability of effective treatment as well as patient's acceptance. Although some behavioral treatments and therapies for alcoholism are available but their success rate is still moderate and largely depends on timely diagnosis of AUD which is a very challenging task [8]. The American Psychiatric Association (APA) issued the 5th edition of the Diagnostic and Statistical Manual of Mental Disorders (DSM–5) in May 2013, which replaced the earlier criteria of identifying alcohol dependence of a person as described in DSM-4 and combined alcohol abuse and alcohol dependence in only one category of alcohol use disorder (AUD). A person can be diagnosed as an AUD patient (AUD-P) if meeting any two of the 11 criteria as described in DSM-5 during the same 12-month period. These criteria are based on the amount, frequency and control of alcohol consumption, continued intake even after having adverse effects on health as well as social relations along with withdrawal symptoms [9].

Generally, the evaluation of AUD is performed using questionnaires such as AUDIT (Alcohol Use Disorder Identification Test) [10], CAGE (Cutting down, Annoyance by criticism, Guilty feeling, and Eye-openers questions) [11] etc. However, due to the subjectivity of these techniques, it may

Manuscript received November 3, 2020; revised February 17, 2021 and April 10, 2021; accepted April 21, 2021. Date of publication April 26, 2021; date of current version May 4, 2021. This work was supported in part by the Ministry of Higher Education Malaysia under Higher Institutional Centre of Excellence (HICoE) scheme Awarded to the Centre for Intelligent Signal and Imaging Reseacrh (CISIR) and in part by the Yayasan Universiti Teknologi PETRONAS under Grant YUTP-FRG 015LC0-031 and Grant YUTP-FRG 015LC0-292. *(Corresponding author: Norashikin Yahya.)*

This work involved human subjects or animals in its research. Approval of all ethical and experimental procedures and protocols was granted by the Ethics Committee of University Malaya, Malaysia.

Danish M. Khan is with the Centre for Intelligent Signal and Imaging Research (CISIR), Electrical and Electronic Engineering Department, Universiti Teknologi PETRONAS, Seri Iskandar 32610, Malaysia, and also with the Department of Electronic and Telecommunications Engineering, NED University of Engineering and Technology, Karachi 75270, Pakistan.

Norashikin Yahya, Nidal Kamel, and Ibrahima Faye are with the Centre for Intelligent Signal and Imaging Research (CISIR), Electrical and Electronic Engineering Department, Universiti Teknologi PETRONAS, Seri Iskandar 32610, Malaysia (e-mail: norashikin_yahya@utp.edu.my).

Digital Object Identifier 10.1109/TNSRE.2021.3075737

not provide factual indication of an individual's condition. For example, many AUD patients are less truthful, some are unable to precisely define a measure of their alcohol consumption while others are in a state of denial [12]–[14]. Hence, there is a possibility of misjudged assessments when using questionnaire-based techniques in assessing accurate measure of alcohol consumption. Given the fact that the conventional screening methods for AUD-P are subjective and manual, there is a need for more objective methods for automatic screening of AUD [15]–[17].

It is established that excessive alcohol consumption tends to alter human brain's structure and functions. For instance, alcohol acts on multiple ionotropic and metabotropic receptors of inhibitory GABA and excitatory glutamate neurotransmitters [18]. Apart from this, it also affects dopamine which is considered to be a vital neurotransmitter that regulates human's pleasure experience [18]. Although, alcohol addiction could be at least in part due to this imbalance between inhibitory and excitatory system along with damage of neuronal synapses [15], [19], the actual underlying mechanism is still unknown [2].

Neuroimaging modalities such as electroencephalography (EEG) records the synchronous activities of neurons over the cortical area of the brain. The recorded data can be used for development of objective diagnosis of various brain diseases and disorders, specifically, AUD [15]. Recently, machine learning techniques including but not limited to support vector machines (SVMs) and neural network (NN) are used for diagnosis of AUD either directly from EEG signals or from its extracted features such as wavelet transform includes power spectrum of Haar-mother wavelet coefficients [20], energy of coefficients obtained from wavelet packet decomposition (WPD) [21], [22], power spectrum of five different frequency bands (delta, theta, alpha, beta and gamma) [23] etc. Notably, results of the study in [23], showed increase in power of theta and delta rhythms in AUD patients, while there is decrease in power of alpha rhythms normal EEG signal.

A classification algorithm based on machine learning techniques using quantitative electroencephalography features, such as absolute power and relative power was proposed in [24] for automatic diagnosis of AUD. In [25], autocorrelation reflection coefficients have been used as features to discriminate between EEG recorded from AUD-P and healthy subjects. Another scheme to categorize AUD-P and normal EEG signals, on the basis of features extracted from EEG visual evoked potential and trained on a neural network, was proposed in [26]. In [27], Palaniappan proposed a method that uses low, mid and high gamma bands of EEG signals to distinguish chronic AUD-P EEG signals from non-chronic AUD-P signals. The later trend of EEG based classification was using features including signals relative energy [22], entropy [28], and time–frequency images.

Recently, AUD clinical symptoms have been linked with various EEG features such as synchronization likelihood (SL), inter-hemispheric coherence and phase delays [29]. Based on these features, functional influence among different brain regions were used in [15], [30], [31] to find differences between AUD-P and healthy control (HC) subjects. A significant difference has been observed in the neuronal synchronization amongst AUD-P and healthy controls. However, contradictory findings have also been reported in terms of inter-hemisperic coherence where significant reduction in EEG power, phase synchronization and coherence in AUD-P as compared with HC were observed [32]. In contrast, Michael *et al.* in [33] reported an increase in inter-hemispheric coherence. Currently, different classification techniques are being used to automatically diagnose alcoholism. W. Mumtaz *et al.* used machine learning on quantitative electroencephalography (QEEG) features for automatic classification of AUD-P disorders [24]. N Sriraam in [34], proposed a neural network based on spectral entropy of EEG signals to identify AUD-P. A detailed review on EEG based diagnosis of alcoholism is available in [35], [36]. For the detection of alcoholism, usage of deep learning techniques is not widely available in literature. In 2019, a combination of long short-term memory (LSTM) and SVM is used for training over EEG peak visualization method (PVM) from alcoholic and healthy control data [37]. Here, LSTM first extract the features and then trained on SVM producing 90.97% classification accuracy. Recently, a simple LSTM network is used for the classification of alcoholic and non-alcoholic subjects using raw EEG signal [38]. The authors claimed that they are the first to use a deep learning model for the detection of alcoholism and achieved a classification accuracy of 93%. However, regardless of selected features and classification techniques, none of the proposed methods have achieved perfect diagnosis of AUD.

Furthermore, various studies in [29], [39]–[41] have shown significant variation in different features obtained from resting-state EEG of AUD and healthy subjects. Analysis of resting-state EEG may be helpful in monitoring different brain disorders [42] as it may be correlated with maintenance and stability of brain's functional organization [43], [44]. In terms of connectivity, there are several key resting-state networks including the default mode network (DMN) and networks of different components related to sensory, motor, executive control, visual components, frontal, parietal, auditory, temporal and parietal. Amongst these networks, DMN is the highly active network [43] as compared to others which makes DMN as the key contributor in maintaining brain's functional organization.

This paper presents a new biomarker that can potentially be used to indicate the physiological changes occurring in human brain due to excessive alcohol consumption. These variations are observed as a result of exchanged causal effects between different DMN regions. The causal effect of one region on another is defined as brain effective connectivity. The effective connections from all over the DMN regions are fed into a 3D Convolutional Neural Network (CNN) for classification of AUD-P vs. HC subjects.

The rest of this paper is structured as follows: Section II describes the resting-state network specifically, the DMN component in detail and highlights various regions involved in DMN and their mapping to EEG electrodes. Subsequently Section III defines the principles of effective connectivity. Section IV covers the description of Partial Directed Coherence(PDC) algorithm for estimation of EC. It further describes

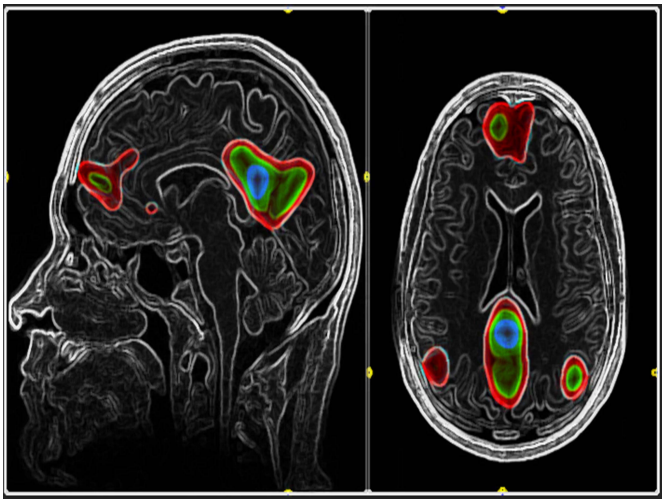

Fig. 1. DMN regions' activation in axial and sagittal view (reproduced from [45]).

TABLE I
BRODMANN AREAS REPRESENTING DMN REGIONS AND CORRESPONDING EEG ELECTRODES

DMN region	Brodmann Area (BA)	EEG Electrode
Precuneus	BA07	Pz
MPC	BA08/09	Fz
MPC	BA08/09L	F3
MPC	BA08/09R	F4
LPC	BA39/40L	P3
LPC	BA39/40R	P4

R= right hemisphere, L = left hemisphere

the experimental and data acquisition set-up along with the code implementation. Section V presents the results and discussion. Finally, section VI concludes the paper.

II. DEFAULT MODE NETWORK

Amongst the Resting-State Networks (RSNs), Default Mode Network (DMN) is often selected for various research works on neurological disorders [46]–[50]. The DMN is identifiable in three regions: (1) precuneus/posterior cingulate, (2) lateral parietal cortex (LPC), and (3) mesial prefrontal cortex (MPC) as shown in Fig. 1. The Brodmann areas for DMN regions along with the nearest electrodes for EEG recording [51], [52] are shown in Table I.

It has been observed that DMN is largely active during resting-state and relatively deactivated during attention-driven tasks such as those requiring frequent use of working memory and visuo-spatial abilities [47], [53]. This means that the activation process of the DMN regions tends to be negatively correlated with regions of elevated activation during tasks [54]–[56]. However, recent studies have also found that DMN exhibits an increased activation when performing particular tasks. For example, Hampson *et al.* in [57] have shown functional connections between precuneus and the mesial frontal gyrus during resting-state as well as during an active-working memory task. This suggests that DMN is not completely inactive during tasks rather it presumably regulates the performance of active tasks [57]. Consequently, a significant relationship between DMN connectivity and behavior suggests that the study of functional or effective connectivity among the DMN regions might be a valuable tool for investigating their deviation from normal conditions. Clinically, this means that if the effective or functional connectivity between DMN regions is used as a biomarker for a particular cognitive disability, diagnosis of different neurological disorders may be performed based on the existence and strength of this connectivity.

Studies related to connectivity between the DMN components have demonstrated that there is strong correlation activation between precuneus or posterior cingulate with the MPC and the lateral parietal region [46], [58]. The precuneus or posterior cingulate plays an essential role since it is directly related to other nodes in the network. Accordingly, it is presumed that precuneus also regulates intrinsic connectivity across these regions. This might be due to the fact that it is amongst the most intensively interconnected regions in the brain [59], [60]. Study by Bukner *et al.* in [46], has supported this interpretation which viewed the precuneus as an essential component for introspective processes as well as for awareness.

III. EFFECTIVE CONNECTIVITY

Brain networks are formed when neurons from different brain regions interact dynamically by regulating and synchronizing their rhythms with one another [61]. The analysis of this interaction is possible either through functional- or effective connectivity techniques. Even though functional connectivity (FC) is capable of determining significant connections efficiently by using cross correlation and mutual information [62], yet, it does not have the ability to identify the direction of influence. This implies that for two brain regions A and B, FC can only provide connections between them, however, any amount of information sent from A to B or vice versa cannot be determined. Moreover, it also incurs third-party effects, i.e. if a region C is affecting region A and B while there is no information transfer happening between A and B themselves, then FC would not only display it as a connection between C & A and C & B but would also show connection between A & B.

Nevertheless, these constraints in FC can be overcome by considering causal interactions between brain regions in lieu of cross-correlation. Such an interaction is referred to as effective connectivity (EC) [63]. It determines the causal influence that one brain region exerts over another as well as provides the direction of influence [64]. Granger causality (GC) is the conventional technique for calculating EC. It states that: A signal (Sig-1) is said to cause another signal (Sig-2) if the latter can be successfully predicted from past values of Sig-1 better than the prediction of Sig-2 from its own past values alone [64]. GC was initially used for prediction of causality of bivariate signals in time domain. However, in [65] Gweke extended its application in frequency domain wherein

he demonstrated how various EEG frequency bands interacted and analysis of coupling between these bands was also made possible. This work holds utmost bio-medical significance and later, GC was altered to fit multivariate signal analysis [65], [66] as well. Presently, directed transfer function (DTF) [67] and PDC [68] techniques are two frequently used variants of GC. In this study, EC has been estimated using PDC since it can efficiently determine connectivity between two brain regions as well as eliminates the third-party effect. PDC is described in the Section IV-A.

IV. Materials and Methods

A. Partial Directed Coherence (PDC)

The general pipeline to automatically classify and diagnose AUD using EC of EEG signals via 3D CNN is shown in Fig. 2. Firstly, signals from 19 electrodes undergo the cleaning process via automatic artefact removal which is described in Section IV-E. Subsequently, S_T continuous segments of length 2-sec are extracted for each subject to calculate PDC. It is important to mention here that the brain is highly dynamic in nature, and, therefore, it is critical to decide appropriate length of the EEG segments to ensure reliable calculation of multivariate autoregressive model (MVAR) modelling parameters. Usually, to ensure the stationarity of an EEG signal, segments of length less than 4-sec are used [69], [70]. In this study, PDC is estimated using different durations such as 2, 3, 4, 5 and 6 seconds to observe the effect of signal length on AUD diagnosis, however a continuous 2-sec segments were selected for the calculation of one PDC matrix due to the fact that it gives large number of samples for the training and testing of 3D-CNN. Subsequently, for each subject, S_T connectivity matrices of 19 channels were obtained. This PDC computation will give a $19\times19\times64$ connectivity matrix at the output which will then be reduced to $6\times6\times64$ connectivity matrix by DMN extraction. The concept of PDC, and the methodology adopted to compute EC as well as the training and testing of 3D-CNN for classification of AUD-P vs. HC are explained in the subsequent sections. MATLAB [71] is used as the programming environment in this study.

PDC is a frequency domain EC technique which is based on the MVAR modelling and partial coherence. Consider a set of κ simultaneously observed time series

$$Y(t) = [y_1(t), y_2(t), \ldots, y_\kappa(t)]^T, \tag{1}$$

denoted by an autoregressive model of order ρ as given in (2)

$$y(t) = \sum_{\tau=1}^{\rho} \mathbf{A}_\tau \mathbf{y}(t-\tau) + \boldsymbol{\epsilon}(t). \tag{2}$$

where $\epsilon(t) = \left[\epsilon_1(t) \cdots \epsilon_\kappa(t)\right]^T$ is zero-mean multivariate gaussian white process and $\mathbf{A}_\tau$ is a $\kappa\times\kappa$-coefficient matrix At time lag τ given by

$$\mathbf{A}_\tau = \begin{bmatrix} a_{11}(\tau) & \cdots & a_{1\kappa}(\tau) \\ \vdots & \ddots & \vdots \\ a_{\kappa 1}(\tau) & \cdots & a_{\kappa\kappa}(\tau) \end{bmatrix}, \tag{3}$$

Algorithm 1 DMN Connectivity Extraction

```
ψ_DMN ← [0]_{6×6×64}
ψ_ALL ← [PDC]_{19×19×64}
ELEC_ALL ← 19 − electrode all combinations
ELEC_DMN ← Electrodes ↦ DMN regions
for all Rows(R) of ψ_ALL do
  for all Columns(C) of ψ_ALL do
    if ELEC_ALL(RC) ∈ ELEC_DMN then
      ψ_DMN(R1, C1) ← ψ_ALL(R, C)
      R1 ← R1 + 1
      C1 ← C1 + 1
    else
      next iteration
    end if
  end for
end for
```

The MVAR coefficient $a_{\mu\nu}$ represents the effect of time-series signal $y_\nu(t-\tau)$ on $y_\mu(t)$.

If $\mathbf{A}(f)$ is the frequency domain equivalent of coefficient matrix $\mathbf{A}_\tau$, then the Fourier transform of $a_{\mu\nu}(\tau)$ can be obtained as,

$$a_{\mu\nu}(f) = \sum_{\tau=1}^{\rho} a_{\mu\nu}(\tau)\, e^{-i\left(\frac{2\pi}{\rho}\right)\tau f} \tag{4}$$

where ν is the source and μ is the sink. Thus, the direction of the influence is $\mu \leftarrow \nu$. $\bar{\mathbf{A}}(f)$ can be obtained by subtracting $\mathbf{A}(f)$ from κ-dimensional identity matrix I, then the PDC, denoted by $\psi_{\mu\nu}(f)$, from electrode ν to electrode μ, is

$$\psi_{\mu\nu}(f) = \frac{\bar{a}_{\mu\nu}(f)}{\sqrt{\bar{a}_\nu^H(f)\,\bar{a}_\nu(f)}}, \tag{5}$$

where $\bar{a}_{\mu\nu}(f)$ denotes the $\mu\nu^{th}$ elements of matrix, and $\bar{\mathbf{A}}(f)$, and $(.)^H$ represent the conjugate transpose. The strength of causal influence of electrodes ν over μ is is given by $\psi_{\mu\nu}(f)$ at frequency f in a normalized range of 0 to 1. The basic MATLAB code for the calculation of PDC is available at [72].

B. Effective Connectivity in Default Mode Network

Based on Brodmann areas (BA) as shown in Table I, six electrodes namely,Pz, Fz, F3, F4, P3, and P4, that constitutes DMN are selected in order to extract $6\times6\times64$-DMN connectivity from $19\times19\times64$-PDC matrices. This procedure of extraction is shown in Algorithm 1. The algorithm takes PDC based EC information for 19 channels as the input and undergoes DMN extraction. This step reduces the size of the $19\times19\times64$-connectivity matrix to $6\times6\times64$. The reduction is performed to remove all the indirect causal effects of non-DMN regions over DMN regions. The third dimension of the EC matrix represents 64-frequency bins equally dividing the frequency range of 0-40 Hz. Thus, each slice of the 3D matrix represents the connectivity between the electrodes at a certain frequency bin. It is noteworthy to mention here that the presence of various artefacts in EEG signals affects the availability of 2-sec continuous segments. Consequently,

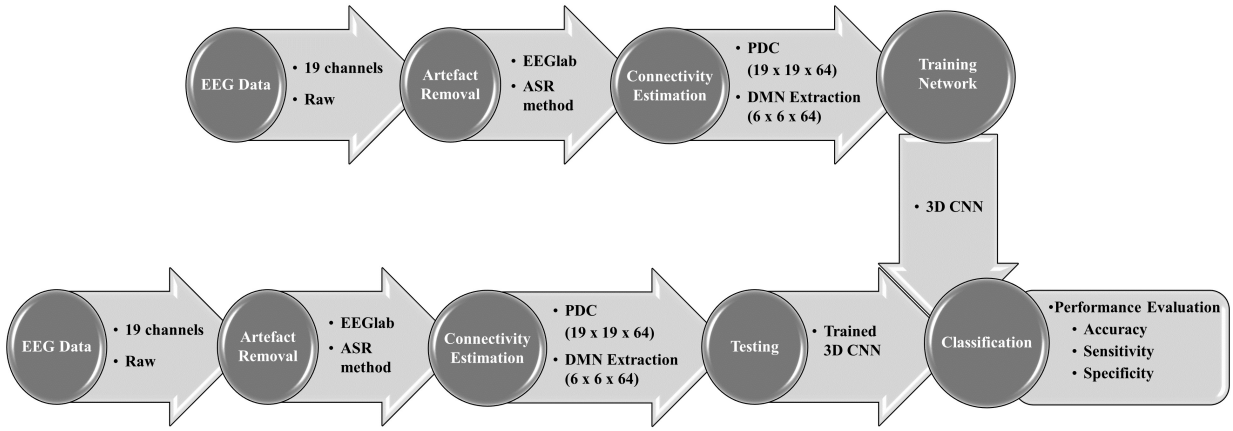

Fig. 2. General pipeline for classification of AUD-P vs. HC using DMN EC.

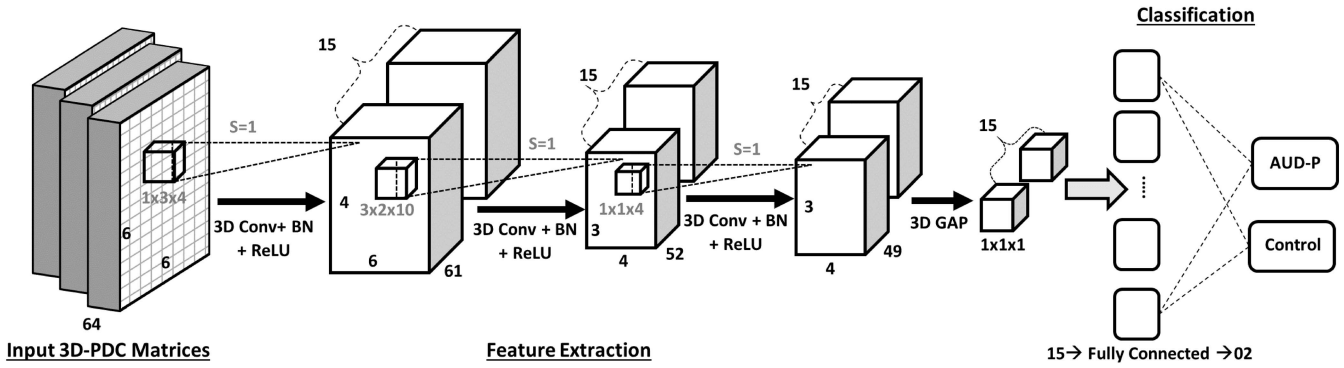

Fig. 3. 3D-CNN architecture for feature extraction and classification of PDC matrices for AUD-P vs. HC. Channel dimensions are represented in grey colour and 3D dimensions are in black. S = Stride, Conv = Convolution, 3D GAP = 3D global average pooling layer.

the total number of PDC matrices S_T varies from subject to subject.

C. Convolutional Neural Network

As explained in section IV-B, the structure of the matrix suggests that major information lies in spatial domain instead of time domain since the subject is in resting-state and the features should be spatially extracted. Considering CNN is designed to exploit spatial correlation of a signal, and given PDC matrices contain information in the 3^{rd} dimension as well, the use of 3D-CNN architecture allows the full utilization of the available features in PDC matrices. Figure 3 depicts the general architecture of our proposed 3D-CNN which includes 3 convolutional layers with batch normalization (BN), a global average pooling (GAP), a dropout and one fully connected layer. The Rectified linear unit (ReLU) layer is placed after each convolution layer as a nonlinear activation function [73]. In the end, binary softmax regression is used with a fully connected layer for classification.

As shown in Fig. 3, 3 convolution layers (CL) use 15 filters each, with dimensions of $1 \times 3 \times 4$, $3 \times 2 \times 10$ and $1 \times 1 \times 4$, respectively. Each CL is followed by a batch normalization layer (BNL) to reduce the internal covariance shift. This reduction leads to an improved training speed and lessens chances of over fitting of the data. The output of BNL is then mapped to positive real numbers by using ReLU layer which is used to activate or deactivate a node based on mapped value. The network architecture along with its configuration and other trainable parameters of the proposed network are summarized in Table II.

Mini-batch size of 64 and ADAM optimizer were used for training of the proposed CNN network. Training parameters of the proposed network are used at their default values as follows; The gradient factor is 0.9, squared gradient decay factor is 0.999, denominator offset for ADAM optimizer is 1×10^{-8}, gradient threshold is 1 while initial learning rate is 1×10^{-3}, learn rate drop factor and period is set to 0.4 and 5, respectively. To avoid overfitting the CNN, a constant weight value of 1×10^{-5} for L2 regularization and 20% dropout layer was selected. Lastly, the softmax layer uses cross-entropy (CE) loss function to classify each input to one of the C mutually exclusive classes. For N number of samples CE loss function is given as,

$$loss_{CE} = -\sum_{i=1}^{N}\sum_{j=1}^{C} x_{ij} \ln y_{ij} \ , \tag{6}$$

where x_{ij} indicates the i^{th} sample belongs to the j^{th} class, and y_{ij} is the output for sample i for class j, i.e., the value

TABLE II
PROPOSED 3D-CNN NETWORK ARCHITECTURE, CONFIGURATION AND TRAINABLE PARAMETERS

Layer	Size	Trainable Parameters
3-D image input	Input Size : 6 × 6 × 64 × 1 Features : 6 × 6 × 64 × 1 = 2304	⊗
Convolution	15 @ (1 × 3 × 4), No Pad,Stride 1, BNL, ReLU	Weights : 1 × 3 × 4 × 1 × 15 = 180 Bias : 1 × 1 × 1 × 15 = 15 Total Parameters : 180 + 15 = 195
Convolution	15 @ (3 × 2 × 10), No Pad,Stride 1, BNL, ReLU	Weights : 3 × 2 × 10 × 15 × 15= 13,500 Bias : 1 × 1 × 1 × 15 = 15 Total Parameters : 13500 + 15 = 13,515
Convolution	15 @ (1 × 1 × 4), No Pad,Stride 1, BNL, ReLU	Weights : 1 × 1 × 4 × 15× 15 = 900 Bias : 1 × 1 × 1× 15 = 15 Total Parameters : 900 + 15 = 915
Global Average Layer	Output : 1 × 1 × 1 × 15	⊗
Dropout	Probability = 0.2	⊗
Fully Connected	Input = 15, Output = 2	Weights : 2 × 15 = 30 Bias : 2 × 1 = 2 Total Parameters : 30 + 2 = 32
Softmax	⊗	⊗
Classification	CE	Total Parameters: 195 + 13515 + 915 + 32 = 14,657

from the softmax function. In CE loss function, the probability of each prediction is compared with the actual class desired output and a penalty term is added based on the difference between two values. This will act as a model weights tuner during training with the goal to minimize this loss for better training. Training is performed by utilizing a GPU (Nvidia Quadro K620) for 100 epochs. The total training time is only about 9.75 min. The proposed 3D-CNN framework can also be used for other neuroscience applications due to its high accuracy and fast training time.

D. Study Participants

In this study the EEG data used comprises 31 AUD-P and 31 HC subjects. The experimental design is approved by the ethic committee of University Malaya, Malaysia. The AUD-P are right-handed 25 Males and 6 Females with average age of 55.2 years and standard deviation of 12.8. Similarly, the control subjects are age-matched (48 ± 10.3), right-handed 20 Males and 11 Females. The AUD-P subjects are the ones meeting the DSM-IV criteria for alcohol dependence and alcohol abuse. All subjects are required to sign consent forms. Exclusion criteria are either those who are under 18 years of age, addicted to other substances than alcohol, have medical and psychiatric problems, are allergic to diazepam, or have refused to sign consent form.

E. EEG Data Acquisition, Pre-Processing and Artefact Removal

Data acquisition for all AUD-P and 15 HC subjects was performed at University Malaya Medical Center (UMMC) and Bingkor Clinic in Kota Kinabalu, Sabah, Malaysia. The data of the remaining 16 HC was recorded at Universiti Teknologi PETRONAS, Malaysia. The recorded EEG was obtained for a duration of 5 minutes under eye-close resting-state condition conducted during morning time in a soundproof room. During the data collection subjects were requested to stay calm and not to move any of their limbs. Two different EEG recording devices, BrainMaster Discovery 24E EEG and the Enobio system, were used in this study with 19 electrodes covering the scalp include FP1, FP2, F3, F4, C3, C4, P3, P4, O1, O2, F7, F8, T3, T4, T5, T6, FZ, CZ, and PZ following the standard 10–20 electrode placement [74]. BrainMaster Discovery uses 256 Hz sampling rate with linked ear as a reference and amplitude in microvolts while Enobio uses 500 Hz sampling rate with mastoid as reference and amplitude in nanovolts. Therefore, in order to normalize the data, EEG recording from the Enobio system was downsampled at 256 Hz and its amplitude was converted to microvolts. Re-referencing of EEG data to Cz was performed for both the devices. A bandpass filter (0.1–70 Hz) and a 50-Hz notch filter were also applied.

The automatic artefact removal was achieved via the EEGLAB software [75], which employs the artifact subspace

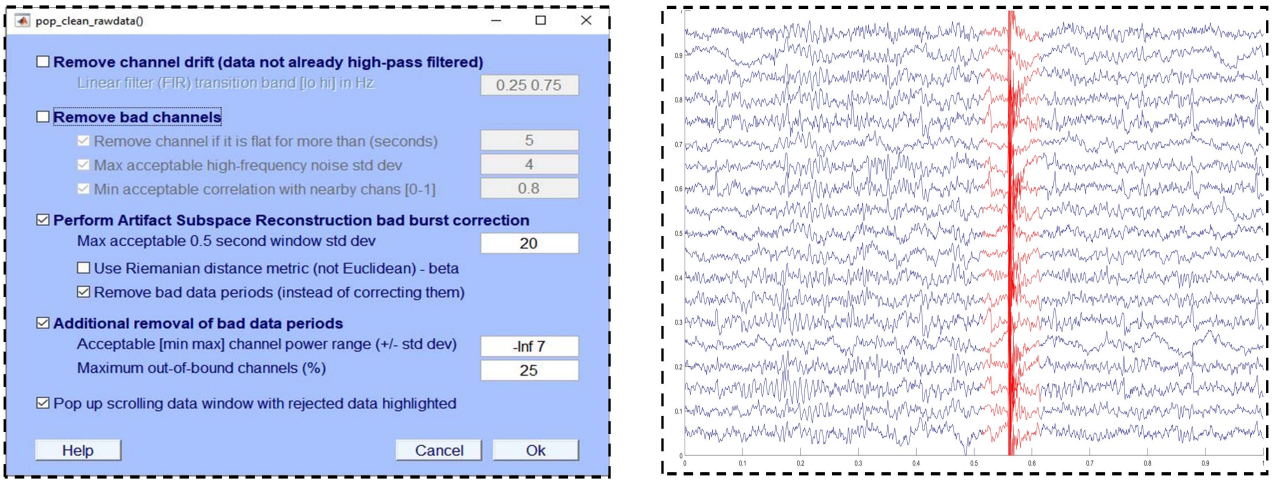

(a) (b)

Fig. 4. Artefact cleaning in EEGlab, showing (a) artefact cleaning parameters and (b) automatic marking of the artefact.

reconstruction (ASR) method to serve the purpose. This built-in plugin detects and removes artefacts resulting from muscle movements, blinking of eyes and other sensory motions by comparing it with artefact free reference data as described in [76]. For cleaning of artefacts, default values provided by EEGLab in the plugin were used. For illustration, Fig. 4 (a) shows a snippet of the toolbox with options for various types of artefacts removal.

Since, our data was already filtered and the bad channels rejection was not needed, these 2 processes were not selected. This gave us marking of bad EEG data as shown in Fig. 4 (b). The data was then analyzed manually in order to check if there were any further remaining artefacts and the boundaries of that portion(s) (if any) were marked. Since, connectivity estimation is susceptible to pre-processing, the data was removed rather than corrected. Based on the boundaries and duration of the artefact, only the data in between was selected. EEG data of a minimum length equal to 2-sec were used after removal of artefacts marked by ASR for calculation of PDC. The data used in this study has been acquired from CISIR's data-repository. It will be made available for use upon reasonable request from the corresponding author after signing a formal data sharing and usage agreement.

F. Classification Algorithm Using CNN

In order to check the generalization and robustness of the proposed network, 5-fold cross-validation (CV) was performed based on 62 subjects such that all PDC samples from each subject are tested at least once with none of its samples presented in training. The average accuracy for each fold iteration is calculated for 10 trials. After k-fold validation and confirmation of generalization, from a total of 31 AUD subjects, 16 were randomly selected for the training phase whereas the remaining 15 were used for testing. Similarly, the 31 HC subjects were also divided into training and testing sets. Accordingly, a total of 4188 (AUD-P = 1959 & HC = 2229) PDC connectivity matrices were obtained for training and 4111 (AUD-P = 1919 & HC = 2192) matrices for testing.Then, as shown in the Fig. 3, all 3D-PDC training matrices were fed to CNN that resulted in a trained network which can classify the unseen test PDC matrices

G. Statistical Analysis

The statistical significance of differences in connectivity between AUD-P and HC was obtained using multivariate analysis of variance (MANOVA) in which a significance level of 0.05 was selected for pairwise comparison. Adjustment for multiple comparison was performed using Bonferroni correction [77].

H. Performance Evaluation

The performance evaluation of the PDC connectivity to distinctly classify AUD-P and HC subjects depends on the performance of the proposed 3D-CNN. If T_P is True Positive, T_N is True Negative, F_P is False Positive, and F_N is False Negative, then the Accuracy (A_{CC}) of the classifier is,

$$A_{CC}\,(\%) = \frac{T_P + T_N}{T_P + T_N + F_P + F_N} \times 100. \tag{7}$$

I. Classification Using Different Brain Rhythms

Neuronal activity in the specific frequency ranges of the brain are associated with different behaviors, states as well as alertness [78]. These frequency ranges are termed as brain rhythms and commonly divided into 5 bands known as delta (δ), theta (θ), alpha (α), beta (β) and gamma (γ). As the PDC matrix contains connectivity over different frequency bands, only the connectivity related to a particular frequency band was used as input to the 3D-CNN network to observe the significance effect of each band in the diagnosis of AUD.

V. Result and Discussion

A. Statistical Significance of Effective Connectivity of DMN

In the first part of this section the variations in the EC values over the DMN electrodes between AUD-P and HC, are established using signal lengths of 2, 3, 4, 5 and 6 and 5-fold cross validation of 3D-CNN is performed as shown in Table III.

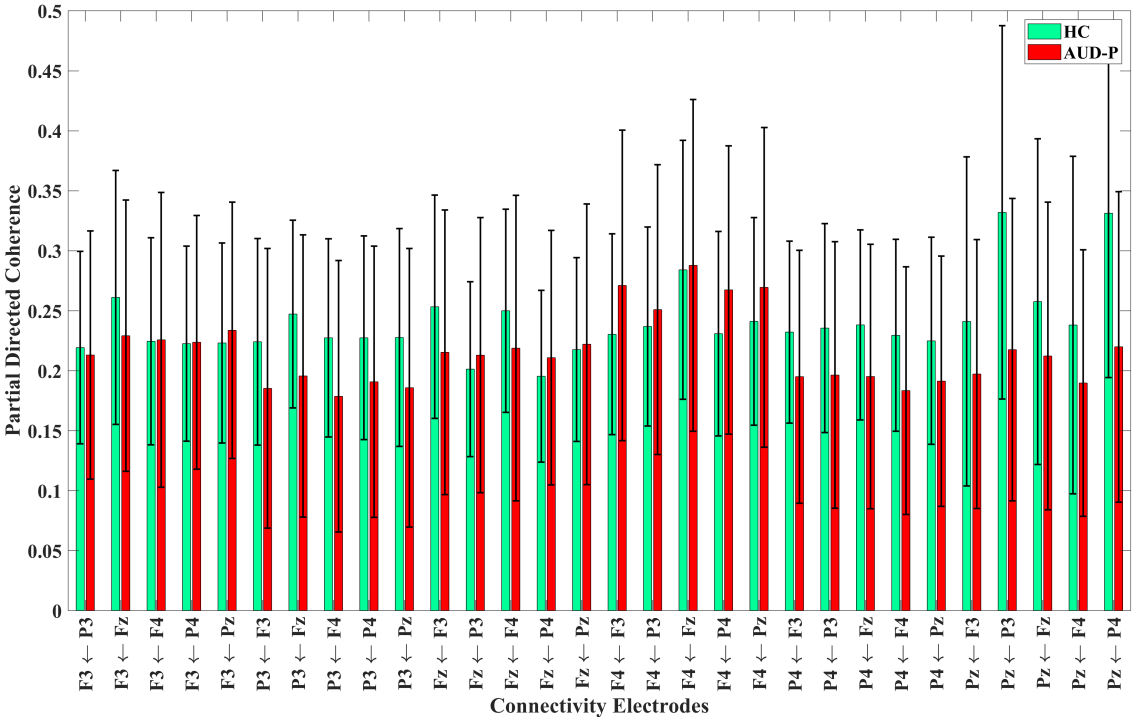

Fig. 5. Average PDC connectivity of DMN electrodes with their standard deviation for 31 AUD-P and 31 HC subjects.

TABLE III
5-FOLD CV ACCURACY USING EC EXTRACTED FROM DIFFERENT LENGTH OF DATA SEGMENT

Segment Duration (sec)	HC A_{CC} (%)	AUD-P A_{CC} (%)	Total A_{CC} (%)
2	90.06 ± 5.31	85.64 ± 6.08	87.85 ± 4.64
3	89.55 ± 6.05	82.27 ± 9.89	86.16 ± 7.33
4	93.1 ± 4.74	85.29 ± 7.31	89.39 ± 5.98
5	92.76 ± 5.62	84.07 ± 4.15	88.81 ± 4.96
6	92.15 ± 6.56	84.83 ± 3.43	88.95 ± 5.02

TABLE IV
SIGNIFICANT CONNECTIONS IN DMN AND THEIR *p*-VALUES

Connections	*p*-Value	Connections	*p*-Value
F3 ← F3	0	F4 ← F4	0
F3 ← Fz	0.012	F4 ← P4	0.009
P3 ← F3	0.011	P4 ← F3	0.002
P3 ← P3	0.003	P4 ← P3	0.002
P3 ← Fz	0.001	P4 ← Fz	0.001
P3 ← F4	0.001	P4 ← F4	0
P3 ← P4	0.005	P4 ← P4	0.01
P3 ← PZ	0.002	P4 ← PZ	0.003
Fz ← F3	0.004	Pz ← P3	0
Fz ← Fz	0.005	Pz ← F4	0.042
Fz ← F4	0.031	Pz ← P4	0
F4 ← F3	0.005	Pz ← PZ	0.003

Table III indicates that classification accuracies obtained using different length of segments are comparable. This may be due to the fact that subjects are in eye-close resting-state which should not be changed drastically over the period of time. However, 2-sec PDC is used for further analysis since it gives the largest number of samples. Bayesian information criterion [79] is used for the calculation of MVAR model order. The average model for AUD-P and HC is found to be 3.02 ± 1.57 and 4.16 ± 0.57, respectively. Calculation of the EC matrices over the six electrodes of the DMN is obtained by averaging over the S_T samples in each subject followed by averaging over all subjects. This averaging process of the PDC estimated EC matrices, is applied separately on AUD-P and HC subjects. The mean strengths of each connection along with the standard deviation within the DMN networks of AUD-P and HC are shown in Fig. 5. From the plot in Fig. 5, it can be seen that the causal effect of the DMN regions on each other is more intense in HC than AUD-P over the majority of the connections. This simply means that the flow of information between the DMN regions and accordingly the mutual influence among these regions is highly involved with HC than AUD-P. In contrast, AUD-P indicates less causal effect in DMN regions which means they are more separated from each other and is in agreement with the findings in [80].

Statistical significance test via MANOVA is applied on the EC of AUD-P vs. HC subjects with significance level set at 0.05. The test has indicated that there are 24 significance ECs at *p*-values less than 0.05 as tabulated in Table IV. These major differences in DMN effective connections between

TABLE V
K-FOLD CV ACCURACY OF PROPOSED 3D-CNN

k-fold CV (k)	HC A_{CC} (%)	AUD-P A_{CC} (%)	Total A_{CC} (%)
2	90.25 ± 9.40	77.75 ± 18.74	83.85 ± 4.59
3	88.53 ± 2.61	80.3 ±11.61	84.42 ± 1.73
4	90.1 ± 3.64	82.13 ± 6.15	86.12 ± 7.39
5	90.06 ± 5.31	85.64 ± 6.08	87.85 ± 4.64

Fig. 6. Confusion matrix generated from 5-fold CV.

AUD-P and HC subjects, give the 3D-CNN the opportunity to produce accurate classification of the AUD.

B. Classification of AUD-P Vs HC Using Effective Connectivity of DMN

The generalization and robustness of the 3D-CNN for all subjects are evaluated using a 5-fold CV. Results of this evaluation are presented in Table V, in terms of averaged accuracy ± standard deviation for each fold and the best 5-fold confusion matrix is shown in Fig. 6. As shown in Table V, high average value of 5-fold accuracy as well as values of each round accuracy confirm the generalization of the model as well as the possibility of using EC within DMN regions as a potential biomarker for the diagnosis of AUD.

The classification of AUD-P vs. HC using EC of DMN is performed by using 3D-CNN architecture and taking advantage of the 3D structure of the PDC matrices. The performance in terms of accuracy is evaluated for each PDC matrix and for each test subject. These results are presented in Table VI for 15 AUD-P and 15 HC subjects. It should be noted that the different number of PDC connectivity matrices, S_T for all subjects, is due to the variability in the number of continuous two seconds segments of EEG recording.

TABLE VI
CLASSIFICATION PERFORMANCE OF 15 AUD-P (TEST SUBJECTS 1 TO 15) AND 15 HC (TEST SUBJECTS 16 TO 30)

Test Subject No	PDC matrices (S_T)	Samples identified as		A_{CC} (%)	Decision
		AUD-P (S_A)	HC (S_H)		
1	127	126	1	99.21	AUD-P
2	139	135	4	97.12	AUD-P
3	148	142	6	95.95	AUD-P
4	127	93	34	73.23	AUD-P
5	147	136	11	92.52	AUD-P
6	147	136	11	92.52	AUD-P
7	129	129	0	100	AUD-P
8	146	146	0	100	AUD-P
9	57	56	1	98.25	AUD-P
10	168	167	1	99.4	AUD-P
11	121	121	0	100	AUD-P
12	157	157	0	100	AUD-P
13	150	141	9	94	AUD-P
14	98	98	0	100	AUD-P
15	58	58	0	100	AUD-P
16	135	15	120	88.89	HC
17	136	26	110	80.88	HC
18	149	8	141	94.63	HC
19	143	14	129	90.21	HC
20	139	15	124	89.21	HC
21	148	7	141	95.27	HC
22	152	11	141	92.76	HC
23	162	6	156	96.3	HC
24	146	4	142	97.26	HC
25	150	5	145	96.67	HC
26	146	10	136	93.15	HC
27	136	7	129	94.85	HC
28	171	32	139	81.29	HC
29	132	26	106	80.3	HC
30	147	37	110	74.83	HC

The classification accuracy based on samples of PDC varies from the lowest value of 73.23% to a perfect score of 100% with average values of 95.9% and 89.8% for AUD-P and HC cases, respectively. The overall average accuracy for classification of the AUD-P and HC PDC matrices is at 92.7%. Detail for classification of the PDC matrices is available in the confusion matrix as shown in Fig. 7.

Referring to Table VI, the performance is subject dependent so there is variation in accuracy for different subjects mainly because EEG signals are known to vary for different subjects [81], [82]. In addition, minor variations in resting-state EC of DMN are expected over the duration of recording which are manifested in the form of mis-classification of PDC matrices in 24 subjects. However, as shown in Table VI,

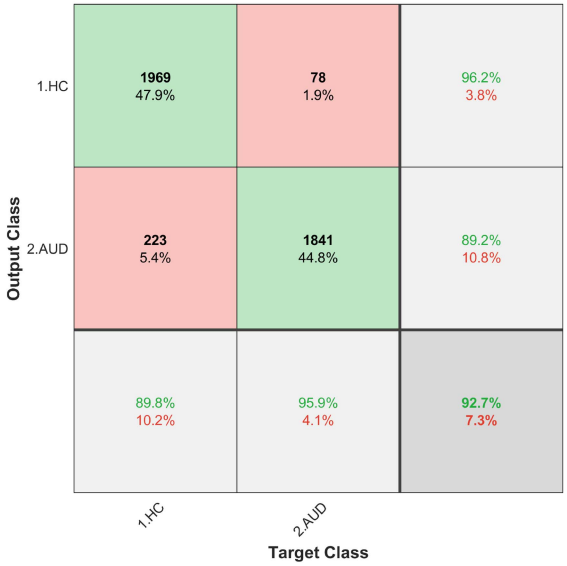

Fig. 7. Confusion matrix for PDC matrices classification of 15 AUD-P and 15 HC test subjects using 3D-CNN.

TABLE VII
5-FOLD CV ACCURACY USING EC OF DIFFERENT BRAIN RHYTHMS

Brain Rhythm	Frequency Range (Hz)	HC A_{CC} (%)	AUD-P A_{CC} (%)	Total A_{CC} (%)
Delta	0 - 4	82.42 ± 7.01	70.84 ± 7.99	77.05 ± 6.97
Theta	4 - 8	84.52 ± 8.4	72.11 ± 9.45	78.83 ± 7.94
Alpha	8 - 12	85.67 ± 7.87	75.86 ± 8.01	81.26 ± 6.66
Beta	12 - 30	88.93 ± 4.44	83.36 ± 7.06	86.16 ± 5.26
Gamma	30 - 40	90.79 ± 3.73	75.64 ± 8.13	83.44 ± 5.51

the classification results obtained from the deep learning network statistically demonstrate better tendency towards the right decision over all the subjects. This can be visualized through the significant gaps between the number of true and wrong classifications within the same subject. Thus, by using (7), all the testing subjects are classified with 100% accuracy.

C. AUD Diagnosis and Brain Rhythms

In order to analyze the contribution of each band in the diagnosis of AUD, the connectivities in the frequency bins of specific brain rhythms are made as the only input to the proposed 3D-CNN network and the classification accuracy achieved via each band is shown in Table VII.

It can be seen in Table VII, delta, theta and alpha bands are not giving good classification accuracies. Notably, moderate classification accuracy is obtained using gamma band while higher ($>85\%$) classification accuracy is obtained using beta band connectivities. This indicates that the resting-state of AUD-P and HC differs significantly in beta and gamma band as observed in various other studies [83]–[85]. To further validate these findings, classification based on combination of delta, theta and alpha as well as combination of beta and gamma band connectivities are performed and is shown in Table VIII.

TABLE VIII
5-FOLD CV ACCURACY USING COMBINATION OF DIFFERENT BANDS

Brain Rhythm	Frequency Range (Hz)	HC A_{CC} (%)	AUD-P A_{CC} (%)	Total A_{CC} (%)
Delta + Theta + Alpha	0-12	85.53 ± 7.2	77.03 ± 11.25	81.77 ± 7.54
Beta + Gamma	12 - 40	90.57 ± 4.57	83.8 ± 11.67	87.31 ± 6.89

Results in Table VIII show that the combination of beta and gamma band connectivities gives high classification accuracy of 87% for samples almost similar to the one obtained while using all bands as demonstrated in Table VI. This suggests that the major contribution in the diagnosis of AUD comes from beta and gamma bands of EEG signals and the EC in these bands can be a potential biomarker in AUD diagnosis.

Recently, machine as well as deep learning techniques have been successfully used to diagnose various brain disorders. Accordingly attempts have also been made to use extracted features from EEG signals for classification of AUD-P and HC. A comparison of the recently published studies based on EEG as input signals to machine- and deep learning techniques are given in Table IX.

It can be observed from Table IX that the detection of alcoholism using EEG has mainly been achieved via machine learning. Besides, a majority of these studies are based on manual feature selection and reduction which itself is a challenging task. Moreover, these methods cannot identify deeply obscured characteristics of EEG signals. Considering the shallow architecture of machine learning with at most a single non-linear feature transformation layer [90], these architectures mostly fail to identify abnormal data points that are present under deep hidden layers [38]. On the other hand, a recent study [38] proposed the use of LSTM network over raw EEG data and introduced the concept of deep learning in the detection of AUD.

In contrast to the aforementioned techniques, our proposed scheme inputs EC to 3D-CNN which gives a classification accuracy of 100% between AUD-P and HC subjects. Moreover, since the technique relies on determining the causal effects between various DMN regions that are fundamentally a resting-state network, therefore, it may be treated as a biomarker for AUD. Furthermore, using the resting-state (RS) to diagnose AUD may not only nullify the differences arising from goal directed tasks due to differences in age, education, gender, physical sloppiness, sensori stimuli disability, interest in task and cognitive disability amongst subjects but would also provide the actual on-going intrinsic activities inside the brain. In particular, RS connectivities between different brain regions could give an informative insight about the pathophysiology of AUD. Apart from these advantages, the proposed AUD diagnosis algorithm inputs only 6 DMN electrodes to the 3D-CNN because of which it is computationally fast. Hence, there is tremendous potential for our proposed technique to be incorporated in clinical investigations of AUD with high

TABLE IX
RECENT AUD DIAGNOSIS METHODS AND THEIR PERFORMANCE COMPARISON WITH THE PROPOSED TECHNIQUE

Ref	Year	Channels	Features	Classification Method	Subject State	No of Subjects		A_{CC} (%)	S_{EN} (%)	SPE (%)
						HC	AUD			
[38]	2020	64	EEG signal	LSTM	Task	45	77	93	N/A	N/A
[86]	2020	64	Wavelet decomposition	Extreme learning machine	VS	Total: 122		87.6	87.37	87.91
[37]	2019	64	EEG PVM	LSTM + SVM	Task	Total: 122		90.97	N/A	N/A
[87]	2019	64	Linear decomposition	Random forest	VS	Total: 122		96.67	N/A	N/A
[88]	2017	19	Relative entropy	KNN (Euclidean)	VS	5	5	80.33	82.67	78
			FC-mutual Information	KNN (Mahalanobis)	VS			82.33	85.33	79.33
[15]	2017	19	FC-SL	SVM	RS	30	30	98	99.9	96.6
[17]	2016	64	Time–frequency images	NNLS classifier	VS	Total: 122		95.83	100	91.67
[24]	2016	19	Absolute and relative power	Logistic model trees	RS	15	30	96	97	93
[89]	2015	19	Absolute power and FC-coherence	LR classifier	RS	15	30	89.3	88.5	91
Proposed Technique	**19 → 6**		**Effective Connectivity (DMN)**	**3D-CNN**	**RS**	**31**	**31**	**100**	**100**	**100**

NNLS = Nonnegative least squares; SL = Synchronization likelihood; LR = Logistic regression; VS = Visual stimuli; RS = Resting-state

degree of reliability; thereby, eliminating subjective nature of questionnaire-based diagnosis.

VI. CONCLUSION

In this paper, the effective connectivity between the DMN regions during the resting-state are estimated using partial directed coherence. The results indicate higher effective connectivity values in the HC subjects than AUD-P for connections between the DMN regions. This indicates more involvement of DMN regions in mutual exchange of information between its regions with HC than AUD-P. Utilizing these major differences in DMN effective connectivity between AUD-P and HC subjects, a deep convolutional neural network is developed for AUD classification. The results show perfect accuracy in identifying AUD-P and HC subjects. Furthermore, it has also been observed that in terms of brain rhythms, beta and gamma bands show significant contribution in AUD diagnosis. Although all the subjects have been correctly classified, due to their limited number, the developed technique needs to be trained and tested with a larger number of subjects before finding its way in clinical tests.

REFERENCES

[1] M. G. Griswold *et al.*, "Alcohol use and burden for 195 countries and territories, 1990–2016: A systematic analysis for the global burden of disease study 2016," *Lancet*, vol. 392, no. 10152, pp. 1015–1035, 2018.

[2] M. Heilig, E. Augier, S. Pfarr, and W. H. Sommer, "Developing neuroscience-based treatments for alcohol addiction: A matter of choice?" *Transl. Psychiatry*, vol. 9, no. 1, pp. 1–11, Dec. 2019.

[3] D. J. Nutt, L. A. King, and L. D. Phillips, "Drug harms in the UK: A multicriteria decision analysis," *Lancet*, vol. 376, no. 9752, pp. 1558–1565, Nov. 2010.

[4] J. Rehm, J. Guiraud, R. Poulnais, and K. D. Shield, "Alcohol dependence and very high risk level of alcohol consumption: A life-threatening and debilitating disease," *Addiction Biol.*, vol. 23, no. 4, pp. 961–968, Jul. 2018.

[5] S. F. Tapert, G. G. Brown, S. S. Kindermann, E. H. Cheung, L. R. Frank, and S. A. Brown, "FMRI measurement of brain dysfunction in alcohol-dependent young women," *Alcoholism, Clin. Experim. Res.*, vol. 25, no. 2, pp. 236–245, Feb. 2001.

[6] A. Priya, P. Yadav, S. Jain, and V. Bajaj, "Efficient method for classification of alcoholic and normal EEG signals using EMD," *J. Eng.*, vol. 2018, no. 3, pp. 166–172, Mar. 2018.

[7] B. F. Grant *et al.*, "Epidemiology of DSM-5 alcohol use disorder: Results from the national epidemiologic survey on alcohol and related conditions iii," *JAMA Psychiatry*, vol. 72, no. 8, pp. 757–766, 2015.

[8] M. Berglund, S. Thelander, and E. Jonsson, *Treating Alcohol and Drug Abuse: An Evidence Based Review*. Hoboken, NJ, USA: Wiley, 2003.

[9] NIH. (2014). *Alcohol Use Disorder: A Comparison Between DSM-IV and DSM-V*. [Online]. Available: https://www.niaaa.nih.gov/publications/brochures-and-fact-sheets/alcoho%l-use-disorder-comparison-between-dsm

[10] S. A. Maisto and R. Saitz, "Alcohol use disorders: Screening and diagnosis," *Amer. J. Addictions*, vol. 12, pp. s12–s25, May 2003.

[11] J. A. Ewing, "Detecting alcoholism: The CAGE questionnaire," *Jama*, vol. 252, no. 14, pp. 1905–1907, 1984.

[12] R. E. Popham and W. Schmidt, "Words and deeds: The validity of self-report data on alcohol consumption," *J. Stud. Alcohol*, vol. 42, no. 3, pp. 355–358, Mar. 1981.

[13] J. Solomon, N. Vanga, J. P. Morgan, and P. Joseph, "Emergency-room physicians': Recognition of alcohol misuse," *J. Stud. Alcohol*, vol. 41, no. 5, pp. 583–586, May 1980.

[14] C. G. Watson, C. Tilleskjor, E. A. Hoodecheck-Schow, J. Pucel, and L. Jacobs, "Do alcoholics give valid self-reports?" *J. Stud. Alcohol*, vol. 45, no. 4, pp. 344–348, Jul. 1984.

[15] W. Mumtaz, M. N. B. M. Saad, N. Kamel, S. S. A. Ali, and A. S. Malik, "An EEG-based functional connectivity measure for automatic detection of alcohol use disorder," *Artif. Intell. Med.*, vol. 84, pp. 79–89, Jan. 2018.

[16] U. R. Acharya, S. V. Sree, S. Chattopadhyay, and J. S. Suri, "Automated diagnosis of normal and alcoholic EEG signals," *Int. J. Neural Syst.*, vol. 22, no. 3, Jun. 2012, Art. no. 1250011.

[17] V. Bajaj, Y. Guo, A. Sengur, S. Siuly, and O. F. Alcin, "A hybrid method based on time–frequency images for classification of alcohol and control EEG signals," *Neural Comput. Appl.*, vol. 28, no. 12, pp. 3717–3723, Dec. 2017.

[18] R. Spanagel, "Alcoholism: A systems approach from molecular physiology to addictive behavior," *Physiolog. Rev.*, vol. 89, no. 2, pp. 649–705, Apr. 2009.

[19] C. L. Ehlers, J. Havstad, D. Prichard, and J. Theiler, "Low doses of ethanol reduce evidence for nonlinear structure in brain activity," *J. Neurosci.*, vol. 18, no. 18, pp. 7474–7486, Sep. 1998.

[20] M. R. N. Kousarrizi, A. A. Ghanbari, A. Gharaviri, M. Teshnehlab, and M. Aliyari, "Classification of alcoholics and non-alcoholics via EEG using SVM and neural networks," in *Proc. 3rd Int. Conf. Bioinf. Biomed. Eng.*, Jun. 2009, pp. 1–4.

[21] A. Yazdani, P. Ataee, S. K. Setarehdan, B. N. Araabi, and C. Lucas, "Neural, fuzzy and neurofuzzy approach to classification of normal and alcoholic electroencephalograms," in *Proc. 5th Int. Symp. Image Signal Process. Anal.*, Sep. 2007, pp. 102–106.

[22] O. Faust, W. Yu, and N. A. Kadri, "Computer-based identification of normal and alcoholic EEG signals using wavelet packets and energy measures," *J. Mech. Med. Biol.*, vol. 13, no. 3, Jun. 2013, Art. no. 1350033.

[23] Y. Sun, N. Ye, and X. Xu, "EEG analysis of alcoholics and controls based on feature extraction," in *Proc. 8th Int. Conf. Signal Process.*, Nov. 2006. [Online]. Available: https://ieeexplore.ieee.org/abstract/document/4128837

[24] W. Mumtaz, P. L. Vuong, L. Xia, A. S. Malik, and R. B. A. Rashid, "Automatic diagnosis of alcohol use disorder using EEG features," *Knowl.-Based Syst.*, vol. 105, pp. 48–59, Aug. 2016.

[25] S. A. Fattah, K. Fatima, and C. Shahnaz, "An approach for classifying alcoholic and non-alcoholic persons based on time domain features extracted from EEG signals," in *Proc. IEEE Int. WIE Conf. Electr. Comput. Eng. (WIECON-ECE)*, Dec. 2015, pp. 479–482.

[26] R. Palaniappan, P. Raveendran, and S. Omatu, "VEP optimal channel selection using genetic algorithm for neural network classification of alcoholics," *IEEE Trans. Neural Netw.*, vol. 13, no. 2, pp. 486–491, Mar. 2002.

[27] R. Palaniappan, "Screening for chronic alcoholic subjects using multiple gamma band EEG: A pilot study," *J. Comput. Sci. Technol.*, vol. 7, no. 2, pp. 182–185, Apr. 2007.

[28] N. Kannathal, U. R. Acharya, C. M. Lim, and P. Sadasivan, "Characterization of EEG-a comparative study," *Comput. Methods Programs Biomed.*, vol. 80, no. 1, pp. 17–23, 2005.

[29] A. Herrera-Díaz *et al.*, "Functional connectivity and quantitative EEG in women with alcohol use disorders: A resting-state study," *Brain Topography*, vol. 29, no. 3, pp. 368–381, May 2016.

[30] E. A. de Bruin, S. Bijl, C. J. Stam, K. B. E. Böcker, J. L. Kenemans, and M. N. Verbaten, "Abnormal EEG synchronisation in heavily drinking students," *Clin. Neurophysiol.*, vol. 115, no. 9, pp. 2048–2055, Sep. 2004.

[31] E. A. de Bruin, C. J. Stam, S. Bijl, M. N. Verbaten, and J. L. Kenemans, "Moderate-to-heavy alcohol intake is associated with differences in synchronization of brain activity during rest and mental rehearsal," *Int. J. Psychophysiol.*, vol. 60, no. 3, pp. 304–314, Jun. 2006.

[32] G. V. Tcheslavski and F. F. Gonen, "Alcoholism-related alterations in spectrum, coherence, and phase synchrony of topical electroencephalogram," *Comput. Biol. Med.*, vol. 42, no. 4, pp. 394–401, Apr. 2012.

[33] A. Michael, K. A. H. Mirza, C. R. Mukundan, and S. M. Channabasavanna, "Interhemispheric electroencephalographic coherence as a biological marker in alcoholism," *Acta Psychiatrica Scandinavica*, vol. 87, no. 3, pp. 213–217, Mar. 1993.

[34] T. K. Padma Shri and N. Sriraam, "EEG based detection of alcoholics using spectral entropy with neural network classifiers," in *Proc. Int. Conf. Biomed. Eng. (ICoBE)*, Feb. 2012, pp. 89–93.

[35] U. R. Acharya, V. S, S. Bhat, H. Adeli, and A. Adeli, "Computer-aided diagnosis of alcoholism-related EEG signals," *Epilepsy Behav.*, vol. 41, pp. 257–263, Dec. 2014.

[36] W. Mumtaz, P. L. Vuong, A. S. Malik, and R. B. A. Rashid, "A review on EEG-based methods for screening and diagnosing alcohol use disorder," *Cognit. Neurodyn.*, vol. 12, no. 2, pp. 141–156, Apr. 2018.

[37] A. Fayyaz, M. Maqbool, and M. Saeed, "Classifying alcoholics and control patients using deep learning and peak visualization method," in *Proc. 3rd Int. Conf. Vis., Image Signal Process.*, Aug. 2019, pp. 1–6.

[38] L. Farsi, S. Siuly, E. Kabir, and H. Wang, "Classification of alcoholic EEG signals using a deep learning method," *IEEE Sensors J.*, vol. 21, no. 3, pp. 3552–3560, Feb. 2021.

[39] K.-L. Son *et al.*, "Neurophysiological features of Internet gaming disorder and alcohol use disorder: A resting-state EEG study," *Transl. Psychiatry*, vol. 5, no. 9, Sep. 2015, Art. no. e628.

[40] A. Sion *et al.*, "Resting-state connectivity and network parameter analysis in alcohol-dependent males. A simultaneous EEG-MEG study," *J. Neurosci. Res.*, vol. 98, no. 10, pp. 1857–1876, 2020.

[41] D. M. Khan, N. Kamel, M. Muzaimi, and T. Hill, "Effective connectivity for default mode network analysis of alcoholism," *Brain Connectivity*, vol. 11, no. 1, pp. 12–29, Feb. 2021.

[42] Y. Bai, X. Xia, and X. Li, "A review of resting-state electroencephalography analysis in disorders of consciousness," *Frontiers Neurol.*, vol. 8, p. 471, Sep. 2017.

[43] B. A. Seitzman, A. Z. Snyder, E. C. Leuthardt, and J. S. Shimony, "The state of resting state networks," *Topics Magn. Reson. Imag.*, vol. 28, no. 4, pp. 189–196, 2019.

[44] T. O. Laumann *et al.*, "On the stability of bold fMRI correlations," *Cerebral cortex*, vol. 27, no. 10, pp. 4719–4732, 2017.

[45] N. Challenged. (2015). *Know Your Brain: Default Mode Network*. [Online]. Available: https://www.neuroscientificallychallenged.com/blog/know-your-brain-defa%ult-mode-network

[46] R. L. Buckner, J. R. Andrews-Hanna, and D. L. Schacter, "The brain's default network: Anatomy, function, and relevance to disease," *Ann. New York Acad. Sci.*, vol. 1124, pp. 1–38, 2008.

[47] M. D. Greicius, B. Krasnow, A. L. Reiss, and V. Menon, "Functional connectivity in the resting brain: A network analysis of the default mode hypothesis," *Proc. Nat. Acad. Sci. USA*, vol. 100, no. 1, pp. 253–258, Jan. 2003.

[48] M. E. Raichle, A. M. MacLeod, A. Z. Snyder, W. J. Powers, D. A. Gusnard, and G. L. Shulman, "A default mode of brain function," *Proc. Nat. Acad. Sci. USA*, vol. 98, no. 2, pp. 676–682, 2001.

[49] M. E. Raichle and A. Z. Snyder, "A default mode of brain function: A brief history of an evolving idea," *NeuroImage*, vol. 37, no. 4, pp. 1083–1090, Oct. 2007.

[50] C. Rosazza and L. Minati, "Resting-state brain networks: Literature review and clinical applications," *Neurological Sci.*, vol. 32, no. 5, pp. 773–785, Oct. 2011.

[51] BRMLAB. *Closest 10-10 Electrode Position to Each Brodmann Area*. Accessed: Aug. 17, 2020. [Online]. Available: https://brmlab.cz/project/brain_hacking/broadmannarea

[52] L. Koessler *et al.*, "Automated cortical projection of EEG sensors: Anatomical correlation via the international 10–10 system," *NeuroImage*, vol. 46, no. 1, pp. 64–72, May 2009.

[53] M. Corbetta and G. L. Shulman, "Control of goal-directed and stimulus-driven attention in the brain," *Nature Rev. Neurosci.*, vol. 3, no. 3, p. 201, 2002.

[54] M. D. Fox, A. Z. Snyder, J. L. Vincent, M. Corbetta, D. C. Van Essen, and M. E. Raichle, "The human brain is intrinsically organized into dynamic, anticorrelated functional networks," *Proc. Nat. Acad. Sci. USA*, vol. 102, no. 27, pp. 9673–9678, 2005.

[55] C.-S. R. Li, P. Yan, K. L. Bergquist, and R. Sinha, "Greater activation of the 'default' brain regions predicts stop signal errors," *NeuroImage*, vol. 38, no. 3, pp. 640–648, 2007.

[56] D. H. Weissman, K. Roberts, K. Visscher, and M. Woldorff, "The neural bases of momentary lapses in attention," *Nature Neurosci.*, vol. 9, no. 7, p. 971, 2006.

[57] M. Hampson, N. R. Driesen, P. Skudlarski, J. C. Gore, and R. T. Constable, "Brain connectivity related to working memory performance," *J. Neurosci.*, vol. 26, no. 51, pp. 13338–13343, Dec. 2006.

[58] P. Fransson and G. Marrelec, "The precuneus/posterior cingulate cortex plays a pivotal role in the default mode network: Evidence from a partial correlation network analysis," *NeuroImage*, vol. 42, no. 3, pp. 1178–1184, Sep. 2008.

[59] A. E. Cavanna and M. R. Trimble, "The precuneus: A review of its functional anatomy and behavioural correlates," *Brain*, vol. 129, no. 3, pp. 564–583, Mar. 2006.

[60] P. Hagmann *et al.*, "Mapping the structural core of human cerebral cortex," *PLoS Biol.*, vol. 6, no. 7, Jul. 2008, Art. no. e159.

[61] V. Sakkalis, "Review of advanced techniques for the estimation of brain connectivity measured with EEG/MEG," *Comput. Biol. Med.*, vol. 41, no. 12, pp. 1110–1117, 2011.

[62] H. E. Wang, C. G. Bénar, P. P. Quilichini, K. J. Friston, V. K. Jirsa, and C. Bernard, "A systematic framework for functional connectivity measures," *Frontiers Neurosci.*, vol. 8, p. 405, Dec. 2014.
[63] K. Friston, R. Moran, and A. K. Seth, "Analysing connectivity with Granger causality and dynamic causal modelling," *Current Opinion Neurobiol.*, vol. 23, no. 2, pp. 172–178, 2013.
[64] C. W. Granger, "Investigating causal relations by econometric models and cross-spectral methods," *Econometrica, J. Econ. Soc.*, vol. 37, no. 3, pp. 424–438, Aug. 1969.
[65] J. F. Geweke, "Measures of conditional linear dependence and feedback between time series," *J. Amer. Statist. Assoc.*, vol. 79, no. 388, pp. 907–915, Dec. 1984.
[66] Y. Hosoya, "Elimination of third-series effect and defining partial measures of causality," *J. Time Ser. Anal.*, vol. 22, no. 5, pp. 537–554, Sep. 2001.
[67] M. J. Kaminski and K. J. Blinowska, "A new method of the description of the information flow in the brain structures," *Biol. Cybern.*, vol. 65, no. 3, pp. 203–210, Jul. 1991.
[68] K. Sameshima and L. A. Baccalá, "Using partial directed coherence to describe neuronal ensemble interactions," *J. Neurosci. Methods*, vol. 94, no. 1, pp. 93–103, Dec. 1999.
[69] N. Nicolaou, S. Hourris, P. Alexandrou, and J. Georgiou, "EEG-based automatic classification of 'awake' versus 'anesthetized' state in general anesthesia using granger causality," *PLoS ONE*, vol. 7, no. 3, Mar. 2012, Art. no. e33869.
[70] W. Hesse, E. Möller, M. Arnold, and B. Schack, "The use of time-variant EEG granger causality for inspecting directed interdependencies of neural assemblies," *J. Neurosci. Methods*, vol. 124, no. 1, pp. 27–44, Mar. 2003.
[71] *MATLAB Version 9.8.0.1396136 (R2020a) Update 3*, The Mathworks, Inc., Natick, MA, USA, 2020.
[72] A. Omidvarnia. (Aug. 2020). *Time-Varying Eeg Connectivity: A Time-Frequency Approach*. [Online]. Available: https://www.mathworks.com/matlabcentral/fileexchange/33721-time-varying%-EEG-connectivity-a-time-frequency-approach
[73] A. F. Agarap, "Deep learning using rectified linear units (ReLU)," 2018, *arXiv:1803.08375*. [Online]. Available: http://arxiv.org/abs/1803.08375
[74] J. N. Acharya, A. J. Hani, J. Cheek, P. Thirumala, and T. N. Tsuchida, "American clinical neurophysiology society guideline 2: Guidelines for standard electrode position nomenclature," *Neurodiagnostic J.*, vol. 56, no. 4, pp. 245–252, Oct. 2016.
[75] A. Delorme and S. Makeig, "EEGLAB: An open source toolbox for analysis of single-trial EEG dynamics including independent component analysis," *J. Neurosci. Methods*, vol. 134, no. 1, pp. 9–21, Mar. 2004.
[76] T. R. Mullen *et al.*, "Real-time neuroimaging and cognitive monitoring using wearable dry EEG," *IEEE Trans. Biomed. Eng.*, vol. 62, no. 11, pp. 2553–2567, Nov. 2015.
[77] J. H. McDonald, *Handbook of Biological Statistics*, vol. 2. Baltimore, MD, USA: Sparky House Publishing, 2009.
[78] M. G. Frank, *Brain Rhythms*. Berlin, Germany: Springer, 2009, pp. 482–483, doi: 10.1007/978-3-540-29678-2_727.
[79] G. Schwarz, "Estimating the dimension of a model," *Ann. Statist.*, vol. 6, no. 2, pp. 461–464, Mar. 1978.
[80] Z. Song, J. Chen, Z. Wen, and L. Zhang, "Abnormal functional connectivity and effective connectivity between the default mode network and attention networks in patients with alcohol-use disorder," *Acta Radiologica*, vol. 62, no. 2, pp. 251–259, Feb. 2021.
[81] A. Melnik *et al.*, "Systems, subjects, sessions: To what extent do these factors influence EEG data?" *Frontiers Human Neurosci.*, vol. 11, p. 150, Mar. 2017.
[82] T. Nishimoto, H. Higashi, H. Morioka, and S. Ishii, "EEG-based personal identification method using unsupervised feature extraction and its robustness against intra-subject variability," *J. Neural Eng.*, vol. 17, no. 2, Mar. 2020, Art. no. 026007.
[83] M. Rangaswamy *et al.*, "Beta power in the EEG of alcoholics," *Biol. Psychiatry*, vol. 52, no. 8, pp. 831–842, Oct. 2002.
[84] B. Porjesz and H. Begleiter, "Alcoholism and human electrophysiology," *Alcohol Res. Health*, vol. 27, no. 2, p. 153, 2003.
[85] J. U. Ramlakhan, M. Ma, R. Zomorrodi, D. M. Blumberger, Y. Noda, and M. S. Barr, "The role of gamma oscillations in the pathophysiology of substance use disorders," *J. Personalized Med.*, vol. 11, no. 1, p. 17, Dec. 2020.
[86] E. Malar and M. Gauthaam, "Wavelet analysis of EEG for the identification of alcoholics using probabilistic classifiers and neural networks," *Int. J. Intell. Sustain. Comput.*, vol. 1, no. 1, pp. 3–18, 2020.
[87] T. Rieg, J. Frick, M. Hitzler, and R. Buettner, "High-performance detection of alcoholism by unfolding the amalgamated EEG spectra using the random forests method," in *Proc. 52nd Hawaii Int. Conf. Syst. Sci.*, Jan. 2019, pp. 1–9.
[88] N. Gökşen and S. Arıca, "A simple approach to detect alcoholics using electroencephalographic signals," in *Proc. EMBEC & NBC*. Singapore: Springer, 2017, pp. 1101–1104.
[89] W. Mumtaz, P. L. Vuong, L. Xia, A. S. Malik, and R. B. A. Rashid, "An EEG-based machine learning method to screen alcohol use disorder," *Cogn. Neurodyn.*, vol. 11, no. 2, pp. 161–171, 2017.
[90] L. Deng and D. Yu, "Deep learning: Methods and applications," *Found. Trends Signal Process.*, vol. 7, nos. 3–4, pp. 197–387, 2014, doi: 10.1561/2000000039.